Effect of coupling strength on a two-lane partially asymmetric coupled totally asymmetric simple exclusion process with Langmuir kinetics

Isha Dhiman and Arvind Kumar Gupta*

Department of Mathematics, Indian Institute of Technology Ropar, Rupnagar 140001 Punjab, India

(Received 13 February 2014; published 16 July 2014)

We analyze an open system comprised of two parallel totally asymmetric simple exclusion processes with particle attachment and detachment in the bulk under partially asymmetric coupling conditions. The phase diagrams are obtained using boundary layer analysis of continuum mean-field equations and characterized for different values of lane-changing rates. The structure of the phase diagram remains qualitatively the same as the one in fully asymmetric coupling conditions up to a certain critical order of lane-changing rates, after which significant changes are found in the phase diagram. The effect of system size on the steady-state dynamics has also been examined. To validate theoretical findings, extensive Monte Carlo simulations are carried out.

DOI: 10.1103/PhysRevE.90.012114 PACS number(s): 02.50.Ey, 05.60.−k, 64.60.−i, 05.70.Ln

I. INTRODUCTION

The totally asymmetric simple exclusion process (TASEP) is considered to be a paradigmatic model for self-driven many-particle systems. The recent research to understand such nonequilibrium systems is motivated by their important applications in physics, chemistry, and biology such as kinetics of biopolymerization [1], protein synthesis [2,3], dynamics of motor proteins [4], gel electrophoresis [5], vehicular traffic [6], and modeling of ant trails [7]. In the TASEP, particles move along a one-dimensional lattice obeying a hard-core exclusion principle with certain preassigned rules. This simple model can well describe some of the complex nonequilibrium phenomena such as boundary-induced phase transitions [8,9], phase separation [10], spontaneous symmetry breaking [11], and shock formation [12–14].

The coupling of a one-dimensional TASEP with a particle attachment-detachment process [Langmuir kinetics (LK)] has gained much attention in the past decade. The additional attachment-detachment dynamics violate particle conservation in the bulk. The importance of studying such processes lies not only in understanding nonequilibrium systems but also in the intracellular transport, where processive molecular motors advance along cytoskeletal filaments and attachment-detachment of motors occurs between the cytoplasm and the filament [15]. The steady-state behavior observed by coupling of the TASEP and LK is considerably different from those known in reference models of the TASEP and LK individually. Mirin and Kolomeisky [16] studied the effects of irreversible detachments in a single-channel TASEP. Parmeggiani *et al.* [17] presented a detailed study about the competing dynamics of particle conservation (TASEP) and particle nonconservation (LK) in a single-channel lattice. The distinguishing characteristics of localization of shocks and phase coexistence have also been identified [12,18]. Mukherji and Mishra [19] performed a boundary layer analysis to study bulk and surface transitions in a one-dimensional TASEP with LK.

Looking at the wide occurrence of multichannel transport processes in the real world, it becomes important to study multichannel nonequilibrium systems. In spite of the substantial work done on multichannel TASEPs [20–29], a few studies have been reported in the literature that investigate multichannel TASEPs in the presence of Langmuir kinetics. In this direction, Jiang *et al.* [30] studied a two-lane TASEP with particle creation and annihilation only in one of the two lanes. Moreover, the particles could jump from one lane to another with equal rates (symmetric coupling). In the context of motor protein traffic, Wang *et al.* [31] proposed a two-lane symmetrically coupled TASEP model with LK in both the lanes. Gupta and Dhiman [32] examined a two-channel TASEP model with Langmuir kinetics in both the lanes with lane changing only in one direction. They found that even a small asymmetry in lane-changing rates can produce significant changes in the phase diagram in comparison to the one of a symmetrically coupled system. The appreciable difference in steady-state properties of a two-channel TASEP with LK in two extreme coupling environments, viz., symmetric and fully asymmetric, encourages us to investigate the system in partially asymmetric coupling conditions, in which particles can move between both lanes, but with unequal rates.

II. TWO-LANE MODEL AND HYDRODYNAMIC MEAN-FIELD APPROXIMATION

We define a system of two parallel one-dimensional lattice channels, each with L sites, denoted by A and B, in which particles are distributed under the hard-core exclusion principle (see Fig. 1). For each time step, a lattice site (i,j) $(i = 1,2,3,\ldots,L;\ j = A,B)$ is randomly chosen. The state of the system is characterized by a set of occupation numbers $\tau_{i,j}$ $(i = 1,2,3,\ldots,L;\ j = A,B)$, each of which is either zero (vacant site) or one (occupied site). At the entrance $(i = 1)$ a particle can enter the lattice with a rate α provided $\tau_{1,j} = 0$ and at the exit $(i = L)$ a particle can leave the lattice with a rate β when $\tau_{L,j} = 1$. In the bulk, if $\tau_{i,j} = 1$, then the particle at site (i,j) first tries to detach itself from the system with a rate w_d (detachment rate) and if it fails then it moves forward to site $(i+1,j)$ provided $\tau_{i+1,j} = 0$; otherwise it attempts to shift to the other lane with a rate w_j (lane-changing rate from the jth lane to the other) only if the target site is vacant. In the

*akgupta@iitrpr.ac.in

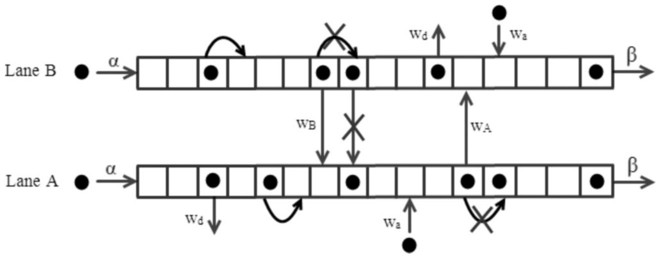

FIG. 1. Schematic diagram of the model. Crossed arrows indicate the forbidden transitions.

bulk, if $\tau_{i,j} = 0$, a particle attaches to the site with a rate w_a (attachment rate).

The proposed model can be thought of as a two-lane asymmetrically coupled TASEP with LK in both the lanes. The rule for an asymmetric lane change between the two lanes imparts to the model its generality over the existing two-lane coupled TASEP models with LK [30–32]. Note that our model is suitable to study a number of two-lane transport processes such as vehicular traffic and motor proteins because normally a vehicle or a molecular motor does not change its lane unless hindered by another one preceding it. This is completely in accordance with the lane-changing rules defined by us.

The temporal evolution of bulk particle densities ($1 < i < L$) in both lanes ($j = A,B$) can be computed from the master equations

$$\begin{aligned}\frac{d\langle\tau_{i,j}\rangle}{dt} &= \langle\tau_{i-1,j}(1-\tau_{i,j})\rangle - \langle\tau_{i,j}(1-\tau_{i+1,j})\rangle\\ &\quad + \omega_a\langle 1-\tau_{i,j}\rangle - \omega_d\langle\tau_{i,j}\rangle\\ &\quad \mp \omega_A\langle\tau_{i,A}\tau_{i+1,A}(1-\tau_{i,B})\rangle\\ &\quad \pm \omega_B\langle\tau_{i,B}\tau_{i+1,B}(1-\tau_{i,A})\rangle, \end{aligned} \tag{1}$$

where $\langle\cdots\rangle$ denotes the statistical average and last two terms on right-hand side take a negative (positive) sign and a positive (negative) sign for lane A (B), respectively. At the boundaries, the particle densities evolve according to

$$\frac{d\langle\tau_{1,j}\rangle}{dt} = \alpha\langle(1-\tau_{1,j})\rangle - \langle\tau_{1,j}(1-\tau_{2,j})\rangle, \tag{2}$$

$$\frac{d\langle\tau_{L,j}\rangle}{dt} = \langle\tau_{L-1,j}(1-\tau_{L,j})\rangle - \beta\langle\tau_{L,j}\rangle. \tag{3}$$

Factorizing the correlations using the mean-field approximation, we get

$$\langle\tau_{i,j}\tau_{i+1,j}\rangle = \langle\tau_{i,j}\rangle\langle\tau_{i+1,j}\rangle. \tag{4}$$

In the hydrodynamic limit $L \to \infty$, we can derive the continuum limit of the model by coarse graining a discrete lattice with lattice constant $\epsilon = 1/L$ and rescaling the time as $t' = t/L$. When the nonconserving processes in the system occur at a comparatively lower rate than particle conserving processes, the system attains a stationary state locally due to conservative dynamics only. Thus, rescaling the time variable is reasonable to understand the engagement between particle conserving and nonconserving dynamics. To observe the competing interplay between the boundary and bulk dynamics, we rescale the attachment, detachment, and lane-changing rates in such a way that the kinetic rates decrease simultaneously with an increase in system size [17]:

$$\Omega_a = \omega_a L, \quad \Omega_d = \omega_d L, \quad \Omega_A = \omega_A L, \Omega_B = \omega_B L. \tag{5}$$

Note that the parameters Ω_a, Ω_d, Ω_A, and Ω_B remain finite in the limit $L \to \infty$.

We replace the binary discrete variables $\tau_{i,j}$ with continuous variables $\rho_{i,j} \in [0,1]$ and retain the terms up to second order in a Taylor series expansion (for a large system, i.e., $L \gg 1$) to obtain

$$\rho_{i,j\pm 1} = \rho_{i,j} \pm \frac{1}{L}\frac{\partial\rho_{i,j}}{\partial x} + \frac{1}{2L^2}\frac{\partial^2\rho_{i,j}}{\partial x^2} + O\left(\frac{1}{L^3}\right). \tag{6}$$

In the absence of any kind of spatial inhomogeneity, we can drop the subscript i. The average densities (ρ_A and ρ_B) in both lanes, which are functions of time t' and quasicontinuous space variable $x \in [0,1]$, describe the state of the system as

$$\frac{\partial\rho}{\partial t'} + \frac{\partial J}{\partial x} = S, \tag{7}$$

where

$$\rho = \begin{bmatrix}\rho_A\\ \rho_B\end{bmatrix},$$

$$J = \begin{bmatrix}-\frac{\epsilon}{2}\frac{\partial\rho_A}{\partial x} + \rho_A(1-\rho_A)\\ -\frac{\epsilon}{2}\frac{\partial\rho_B}{\partial x} + \rho_B(1-\rho_B)\end{bmatrix},$$

and

$$S = \begin{bmatrix}\Omega_a(1-\rho_A) - \Omega_d\rho_A - \Omega_A\rho_A^2(1-\rho_B) + \Omega_B\rho_B^2(1-\rho_A)\\ \Omega_a(1-\rho_B) - \Omega_d\rho_B + \Omega_A\rho_A^2(1-\rho_B) - \Omega_B\rho_B^2(1-\rho_A)\end{bmatrix}.$$

Here S represents the nonconservative terms formed by the combination of lane-changing transitions and Langmuir kinetics. The components of J are the currents in the particle conservation situation in lanes A and B, respectively. In the particular case of $\Omega_B = 0$, the coupling term, arising due to the biased lane-changing rule, acts as a sink for lane A and a source for lane B [32]. This aspect does not hold true for the present general case of $\Omega_{A,B} \neq 0$.

III. STEADY-STATE SOLUTION: BOUNDARY LAYER ANALYSIS

In this section we determine the steady-state solution of the coupled system (7), for which we need to solve the system

$$\begin{aligned}&\frac{\epsilon}{2}\frac{d^2\rho_A}{dx^2} + (2\rho_A - 1)\frac{d\rho_A}{dx} + \Omega_a(1-\rho_A) - \Omega_d\rho_A\\ &\quad - \Omega_A\rho_A^2(1-\rho_B) + \Omega_B\rho_B^2(1-\rho_A) = 0,\\ &\frac{\epsilon}{2}\frac{d^2\rho_B}{dx^2} + (2\rho_B - 1)\frac{d\rho_B}{dx} + \Omega_a(1-\rho_B) - \Omega_d\rho_B\\ &\quad + \Omega_A\rho_A^2(1-\rho_B) - \Omega_B\rho_B^2(1-\rho_A) = 0.\end{aligned} \tag{8}$$

The boundary conditions for the coupled nonlinear system (8) are $\rho_A(0) = \rho_B(0) = \alpha$ and $\rho_A(1) = \rho_B(1) = 1 - \beta = \gamma$. The leading-order terms in the above system play a role similar to that performed by the vanishing viscosity term (regularizing term) in the Burgers equation. Retaining second-order terms in the system ensures the generation of a smooth solution fitting all four boundary conditions. The shocks or boundary layers (if any) are formed over regions of width of $O(\epsilon = 1/L)$, across which a sudden rise or fall in the density profile occurs while the current remains constant. This constancy in current is due to the irrelevance of the particle nonconserving dynamics in the narrow boundary layer or shock region.

To understand the steady-state behavior of the system (7), we employ a boundary layer analysis of the continuum mean-field equations. Being a general scheme to solve the hydrodynamic equation in the thermodynamic limit [33], this approach has been quite successful in explaining the complete rich phase diagrams of the single-channel TASEP with LK [19] and the two-channel TASEP with LK in fully asymmetric coupling conditions [32], respectively. In the thermodynamic limit ($L \gg 1$), the contribution of the regularizing terms is negligible and the major part of the density profile is described by the solution of the system of first-order equations obtained after neglecting second-order terms in the system (7). This solution is known as the outer solution or bulk solution. The omission of the second-order system makes the coupled system overdetermined, due to which the outer solution is unable to meet the boundary conditions at both boundaries simultaneously. This generates the notion of left outer and right outer solutions. The solution satisfying the left (right) boundary condition is known as left (right) outer solution. Since the density profile has to satisfy the boundary condition at other end also, the global solution cannot be given by the outer solution alone. Thus, to satisfy the boundary conditions at both ends, a narrow regime crossing, from left to right, the solution is formed that gives rise to either a boundary layer or a shock in the density profile. This solution is known as the inner solution and is found by ignoring the nonconservative terms in the steady-state system.

A. Outer solution

Now we need to solve the system of first-order coupled ordinary differential equations [taking the limit $\epsilon \to 0$ in the system (8)] to obtain the outer solution in both lanes. Though the elimination of second-order terms simplifies the system, still it cannot be solved analytically because of the coupling terms. Moreover, the system is overdetermined, due to which it cannot fulfill the four boundary conditions simultaneously. These limitations suggest the use of a suitable numerical scheme to get an approximate outer solution of the continuum mean-field equations. The following numerical scheme for jth lane is used to find the outer solution of the continuum mean-field equations

$$\begin{aligned}\rho_{i,j}^{n+1} &= \rho_{i,j}^{n} + \frac{\epsilon}{2}\frac{\Delta t'}{\Delta x^2}\left(\rho_{i+1,j}^{n} - 2\rho_{i,j}^{n} + \rho_{i-1,j}^{n}\right)\\ &\quad + \frac{\Delta t'}{2\Delta x}\left[\left(2\rho_{i,j}^{n} - 1\right)\left(\rho_{i+1,j}^{n} - \rho_{i-1,j}^{n}\right)\right]\\ &\quad + \Delta t'\left[\Omega_a\left(1 - \rho_{i,j}^{n}\right) - \Omega_d\rho_{i,j}^{n}\right.\\ &\quad \left.\mp \Omega_A\left(\rho_{i,A}^{n}\right)^2\left(1 - \rho_{i,B}^{n}\right) \pm \Omega_B\left(\rho_{i,B}^{n}\right)^2\left(1 - \rho_{i,A}^{n}\right)\right]\\ &\quad + O(\Delta t, \Delta x^2). \end{aligned} \tag{9}$$

Here the last two terms take negative (positive) and positive (negative) signs for lane A (B), respectively. The density profiles in the steady state have been obtained by capturing the solution of the above discretized system in the limit $n \to \infty$, which ensures the occurrence of a steady state.

B. Inner solution

To find the inner solution, we introduce a variable $\tilde{x} = \frac{x - x_d}{\epsilon}$, where x_d is the position of the boundary layer. This rescaling leads to the elimination of the source and sink terms in the hydrodynamic equations, which is well justified because particle nonconserving dynamics are irrelevant in regions of width of $O(\epsilon)$. In terms of the variable $\tilde{x}$, the equations governing the inner solution in the thermodynamic limit can be expressed in a concise form ($j = A,B$) as

$$\frac{1}{2}\frac{d^2\rho_{j,in}}{d\tilde{x}^2} + (2\rho_{j,in} - 1)\frac{d\rho_{j,in}}{d\tilde{x}} = 0. \tag{10}$$

Integrating once with respect to $\tilde{x}$, we have

$$\frac{d\rho_{j,in}}{d\tilde{x}} = 2\left(a_j + \rho_{j,in} - \rho_{j,in}^2\right). \tag{11}$$

Here a_j is the constant of integration and is computed from the matching condition of outer and inner solutions.

If we suppose that the boundary layer appears at the right boundary ($x = 1$) for lane j, the matching condition requires

$$\rho_{j,in}(\tilde{x} \to -\infty) = \rho_{j,out}(x = 1) = \rho_{j,o}. \tag{12}$$

Here $\rho_{j,o}$ is value of the left outer solution in lane j at $x = 1$. Clearly, $\rho_{j,o}$ is a function of the system parameters Ω_d and Ω.

Equation (12) gives $a_j = \rho_{j,o}^2 - \rho_{j,o}$, which physically interprets that the current across the inner solution region must be equal to the bulk current entering the region. Solving Eq. (11) after substituting the value of a_j, we obtain the inner solution in lane j given by

$$\rho_{j,in} = \frac{1}{2} + \frac{|2\rho_{j,o} - 1|}{2}\tanh\left(\frac{\tilde{x}}{w_j} + \xi_j\right), \tag{13}$$

where $w_j = \frac{1}{|2\rho_{j,o} - 1|}$ and $\xi_j = \tanh^{-1}(\frac{2\gamma - 1}{|2\rho_{j,o} - 1|})$. The value of ξ_j is computed from the condition $\rho_{j,in}(\tilde{x} = 0) = \gamma$. The left outer solution $\rho_{j,o}$ is a function of the entrance rate α as it respects the left boundary condition. Thus, ξ_j becomes a function of α as well as γ. This dependence of the inner solution on the boundary rates gives rise to a region in $\alpha - \gamma$ in which we get a right boundary layer in lane j with positive slope. This region is a subregion of the low-density (LD) phase and exists for $\gamma > \rho_{j,o}(\alpha)$. The solution given by Eq. (13) is referred to as the tanh $-r$ solution. Here r denotes the right boundary, i.e., $x = 1$. The slope of the boundary layer given by tanh $-r$ is positive, as shown in Fig. 2, curve (iv). As $\tilde{x} \to \infty$, the boundary layer at $x = 1$ saturates to, say, $\rho_{j,s}$. The saturation of the boundary layer is mathematically expressed by the condition $\rho_{j,o}^2 - \rho_{j,o} + \rho_{j,s} - \rho_{j,s}^2 = 0$, which gives $\rho_{j,s} = 1 - \rho_{j,o}$. When $\gamma > \rho_{j,s}(\alpha)$, the inner solution fails to satisfy the right boundary condition $\rho_{j,in}(\tilde{x} \to \infty) = \gamma$ and deconfines from the boundary to enter the bulk of lane j in the form of a shock. Thus $\gamma = 1 - \rho_{j,o}(\alpha)$ acts as a bulk transition line between LD and shock phases. Such a continuous transition is reminiscent of the bulk transition

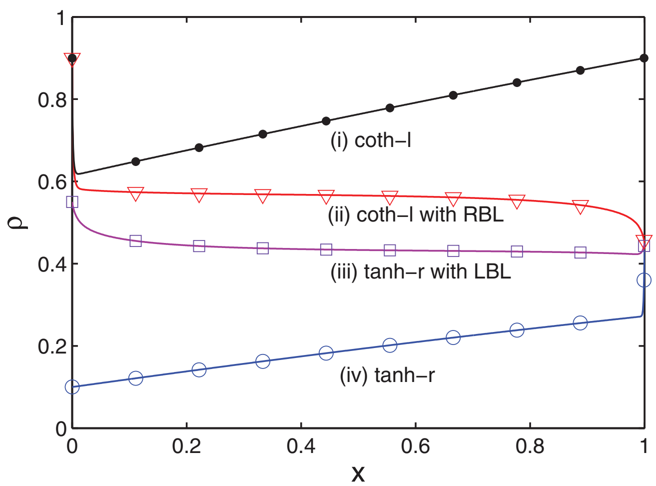

FIG. 2. (Color online) Density profiles showing different kinds of boundary layers: (i) $\alpha = 0.9, \gamma = 0.9$, lane A; (ii) $\alpha = 0.9, \gamma = 0.45$, lane B; (iii) $\alpha = 0.55, \gamma = 0.45$, lane A; and (iv) $\alpha = 0.1, \gamma = 0.45$, lane A.

observed in the single-channel TASEP with LK [19,34], known as a shockening transition. Within the LD phase, the slope of the boundary layer is negative for $\gamma < \rho_{j,o}(\alpha)$ and the inner solution in this region is

$$\rho_{j,in} = \frac{1}{2} + \frac{|2\rho_{j,o} - 1|}{2} \coth\left(\frac{\tilde{x}}{w_j} + \hat{\xi}_j\right), \qquad (14)$$

where $\hat{\xi}_j = \coth^{-1}(\frac{2\gamma-1}{|2\rho_{j,o}-1|})$. This solution is denoted by $\coth -r$. The change in the slope of the boundary layer describes a surface transition, which does not affect bulk density profile. The length scale described by ξ_j shows a logarithmic divergence ($\xi_j \sim \ln|\gamma - \rho_{j,o}|$) as one approaches the surface transition line from either of the two subregions. When $\alpha > 1/2$, a decaying boundary layer starts developing at $x = 0$ and grows in size with an increase in the entrance rate. The appearance of the left boundary layer (LBL) can be understood as follows. In the LD phase, the bulk density is less than 1/2, which is not compatible with the boundary condition $\rho_A(x = 0) = \alpha(>1/2)$. Thus, in order to satisfy the left boundary condition, a decaying boundary layer evolves at $x = 0$. The $\tanh -r$ solution becomes $\tanh - r$ with the LBL [Fig. 2, curve (iii)] as one crosses the vertical line $\alpha = 1/2$ in the phase plane. Along similar lines, we can analyze the boundary layer at $x = 0$.

Importantly, one should not infer from here that the inner solutions in both lanes are independent of nonconservative dynamics. Moreover, the inner solution in lane A is influenced by the inner solution in lane B and vice versa, although this might not appear explicitly by looking at the uncoupled system [Eq. (10)]. However, the lane-changing and attachment-detachment phenomena impart their effect in the inner solution through the matching conditions.

IV. PHASE DIAGRAMS AND THE EFFECT OF LANE-CHANGING RATES

In this section we derive phase diagrams for different values of lane-changing rates and investigate the effect of coupling strength on the steady-state properties. We also validate the numerical solutions of continuum mean-field equations with Monte Carlo simulations for system size $L = 1000$. The Monte Carlo simulations are carried out for 10^{10}–10^{11} time steps and the first 5% of the steps are ignored to ensure the occurrence of a steady state. The densities in both lanes are computed by taking time averages over an interval of $10L$.

It is important to note that the steady-state dynamics of a symmetrically coupled two-lane TASEP with LK are similar to those in a single-lane TASEP with LK (ignoring finite-size effects) [31]. The symmetry in coupling rates leads to the cancellation of lane-changing source terms with sink terms in the mean-field hydrodynamic equations, which gives two uncoupled ordinary differential equations representing two independent TASEPs with LK. Hence, the topology of the phase diagram of the single-lane TASEP with LK model is preserved. This is totally in contrast to the fully asymmetric coupling conditions [32], where we have the existence of another phase diagram, considerably different from that of a single-lane TASEP with LK [17,19].

The two-lane TASEP with LK model has already been analyzed under symmetric [31] and fully asymmetric coupling conditions [32]. Now we consider the important case of partially asymmetric coupling conditions. It has been reported in the literature [20,21,24,29] that the phase diagram of a two-lane TASEP without LK is significantly different in partially asymmetric and fully asymmetric coupling environments. This stimulates the need to answer two important questions: (a) Does there exist any difference in the phase diagrams of a two-lane TASEP with LK under partially asymmetric and fully asymmetric coupling environments? (b) If there are any differences, are they similar to those observed in the corresponding system without LK?

In an attempt to answer the above questions, we investigate the effect of lane-changing rates on the steady-state dynamics of the system. Without any loss of generality, we assume that $\Omega_A > \Omega_B$. We adopt a new terminology to identify the different transition rates. The order of a transition rate Ω_t ($t = a,d,A,B$) is said to be 10^{-m}, denoted by $O(\Omega_t) = 10^{-m}$, if it can be expressed in the form

$$\Omega_t = p * 10^{-m}, \quad p \in [1,10).$$

To begin with, we analyze the case in which the orders of attachment, detachment, and lane-changing rates are consistent. Figure 3 shows the phase diagram for $\Omega_d = \Omega_a = 0.2$, $\Omega_A = 0.8$, and $\Omega_B = 0.2$. In particular, Fig. 3(b) shows the composition of the phase plane on the basis of bulk transitions only, which clearly indicates that there exists six steady-state distinct phases, namely, (LD,LD), (LD,S), (S,HD), (S,S), (HD,HD), and (LD,HD).

On comparing the steady-state phase diagram for $\Omega_A = 0.8$ and $\Omega_B = 0.2$ with that in $\Omega_A = 1$ and $\Omega_B = 0$ [32], the following inferences can be drawn.

(i) There is no qualitative difference in the phase diagram with $\Omega_A = 0.8$ and $\Omega_B = 0.2$ from the one in fully asymmetric

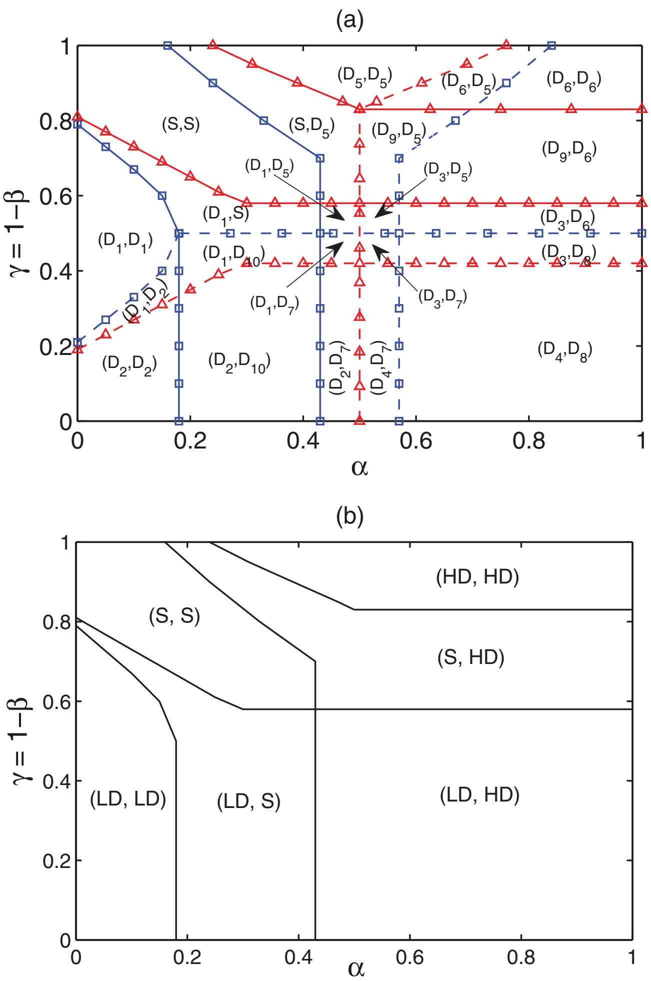

FIG. 3. (Color online) (a) Phase diagram for $\Omega_d = 0.2$, $\Omega_A = 0.8$, and $\Omega_B = 0.2$. The following notation is used: D_1, tanh$-r$; D_2, coth$-r$; D_3, tanh$-r$ with a LBL; D_4, coth$-r$ with a LBL; D_5, tanh$-l$; D_6, coth$-l$; D_7, tanh$-l$ with a RBL; D_8, coth$-l$ with a RBL; D_9, S plus a LBL; and D_{10}, S plus a RBL. Here S denotes shock and LBL and RBL denote the left boundary layer and right boundary layer, respectively. Curves marked with triangles and squares represent phase boundaries of lanes A and B, respectively. Solid and dashed curves denote bulk and surface transitions, respectively. (b) Classification of phases on the basis of bulk transitions only.

coupling conditions. The number of phases also remains conserved.

(ii) When $\Omega_A = \Omega_B$, the phase diagram reduces to the one in the symmetric coupling case and densities in both lanes become equal [31]. The larger the difference is between Ω_A and Ω_B, the greater the deviation is from the phase diagram in symmetric coupling conditions and the greater the density difference is between two lanes. The deviation in the structure as well as the density difference is maximum for fully asymmetric coupling conditions.

(iii) With an increase in $\Omega_A - \Omega_B$, the LD phase in lane A expands while the high-density (HD) phase in lane B shrinks. The reverse phenomenon occurs for phases in lane B. This is due to the increased number of particles shifting from lane A to lane B, which leads to a deficiency and abundance of particles in lane A and lane B, respectively.

(iv) More importantly, the aforementioned observations are true for any values of $\Omega_A \neq \Omega_B$ [provided their magnitude is of $O(\Omega_d)$].

So far, we have investigated the case in which lane-changing rates are of the same order as the attachment and detachment rates. Further, we discuss how the higher orders of lane-changing rates affect the steady-state properties of the system. It is observed that the phase diagram of our system with $O(\Omega_{A,B}) = 10O(\Omega_{a,d})$ has no structural difference from the one with consistent orders. The only noticeable difference is the shifting of various phase boundaries in the phase plane, which leads to a variation in the size of various phases in the phase diagram. For example, the LD phase in lane A (B) expands (contracts) while the HD phase in lane A (B) contracts (expands) with increasing lane-changing rates.

As soon as $O(\Omega_{A,B}) = 100O(\Omega_{a,d})$, the contribution of the attachment and detachment in the system dynamics reduces enough that the behavior of the system is mainly dominated by lane-changing dynamics. A significantly different structure of the phase diagram is obtained as shown in Fig. 4. Figure 4(a) shows a rich and detailed classification of the phase plane into distinct phases generated by bulk as well as surface transitions for $\Omega_A = 80$ and $\Omega_B = 20$. Figure 4(b) represents the composition of the phase plane into six different phases, viz., (LD,LD), (HD,HD), (S,S), (LD,HD), intermediate phase 1, and intermediate phase 2. The division in Fig. 4(b) is on the basis of bulk transitions only.

It is clear from Fig. 4(a) that the phase plane comprises of 18 distinct phases, each of which describes a different density profile. For smaller values of both α and γ, the system is in the LD phase. In the (coth $-$ r,coth $-$ r) phase, the density in both lanes is less than $1/2$ with a coth-type right boundary layer (RBL) at $x = 1$. Fixing α, if one moves in the direction of increasing γ, the coth-type RBL first undergoes a surface transition to the tanh-type RBL, which then deconfines from the boundary to enter the bulk in the form of a shock. The line of deconfinement appears as the phase boundary between the (LD,LD) and (S,S) phases.

For $\gamma < 1/2$, the density in both lanes increases, while the shape of the density profile remains the same on increasing α. As soon as $\alpha \geqslant 0.25$, we enter the intermediate phase in which, up to a certain position in the domain, $\rho_B < 1/2$ and then $\rho_B > 1/2$. Thus, this phase cannot be designated as either (LD,LD) or (LD,HD). An example of the density profile in the intermediate phase 1 is shown in Fig. 5. This phase persists until $\alpha = 0.35$, after which the system is in the (LD,HD) phase. Similar arguments can be given for the transitions from the (HD,HD) phase to the (LD,HD) via the intermediate phase 2 and to the (S,S) phases. In the intermediate phase 2, the density profile in lane A lies neither in the LD nor in the HD phase.

The density profile within the (LD,HD) phase is not of one kind; rather it is classified into nine distinct categories according to the shape of the boundary layer. This particular observation is similar to the phase diagrams for lower orders of lane-changing rates [32].

Now we discuss the three important and distinguishing features of the steady-state phase diagram with $\Omega_A = 80$ and $\Omega_B = 20$.

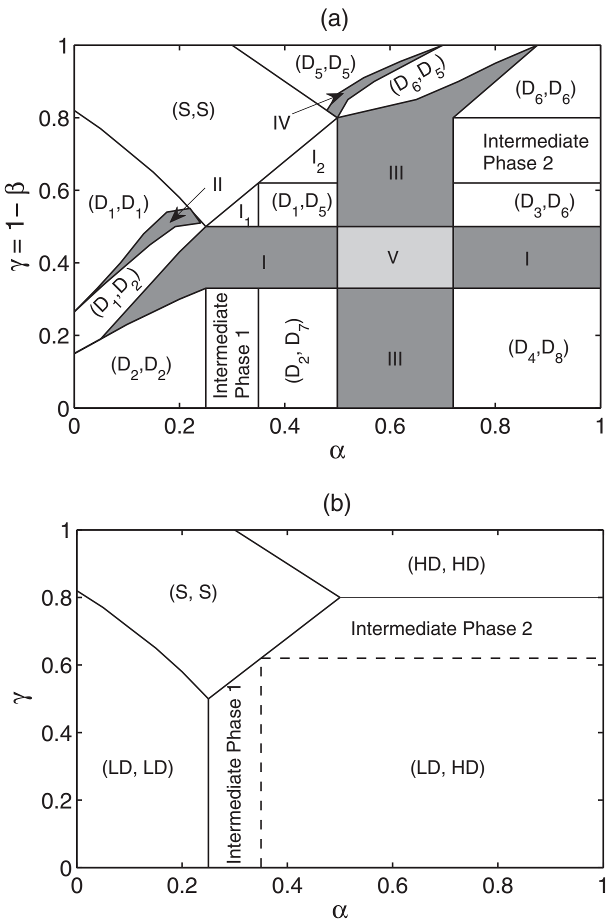

FIG. 4. Phase diagram for $\Omega_A = 80$ and $\Omega_B = 20$. (a) Subregion I shows the downward kink at the RBL in lane A; II, the upward kink at the LBL in lane B; III, the upward kink at the RBL in lane B; IV, the downward kink at the LBL in lane A; V, the intersection region of I and III; I_1, the intermediate phase 1; and I_2, the intermediate phase 2. (b) Classification of phases on the basis of bulk transitions only. The rest of the notation is same as in Fig. 3.

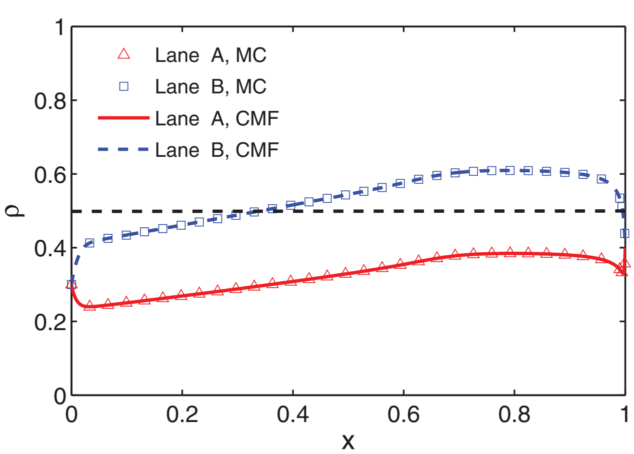

FIG. 5. (Color online) (a) Density profiles in the intermediate phase 1 for $\alpha = 0.3, \gamma = 0.4$. The continuum mean-field density profiles are shown in red (blue) and by a solid (dashed) line in lane A (B). The curve marked with triangles (squares) shows the Monte Carlo simulation results for lane A (B). Clearly, lane A is in the LD phase while lane B is in neither the LD nor the HD phase.

A. Regions of surface transition in the boundary layer

The first important difference in the phase diagram structure of $\Omega_A = 80$ and $\Omega_B = 20$ from the one with lower orders is the appearance of new subregions in the phase plane. So far, we have identified the lines of the surface transition in the LD and HD phases for $O(\Omega_A) = O(\Omega_B) < 100O(\Omega_d)$ that accompany a bulk transition from the LD and HD phases to the shock phase [32]. This surface transition leads to a change in sign of the slope of the boundary layer. In the present case, we obtain regions instead of lines of the surface transition in the LD and HD phases. From Fig. 4(a) one finds the four subregions marked I–IV (shaded), in which the density profile incurs a kink near one of the boundaries. The value of the bulk density is such that the profile of the outer solution cannot meet the inner solution smoothly near the boundary, which leads to the formation of a kink in the density profile. Within the LD phase, subregion I is the region of the surface transition of the RBL in lane A, where the density profile is comprised of a downward kink at the right boundary shown in Fig. 6(a). Similarly, subregion II indicates the surface transition of the right boundary layer in lane B, where the profile at the right boundary shows an upward kink [Fig. 6(b)]. The corresponding regions for the slope change of the left boundary layer in the HD phase are represented by III and IV in lane B and lane A, respectively. It is clear from Fig. 6(c) [Fig. 6(d)] that the LBL in lane B (A) has an upward (downward) kink. Additionally, regions I and IV extend outside the (LD,LD) and (HD,HD) phases, respectively. The density profiles in region V contain a kink at the right boundary layer in lane A and a kink at the left boundary layer in lane B.

B. Synchronization of shocks

Since $\Omega_A > \Omega_B$, the shifting of additional particles from lane A to B creates a relative shortage of particles in lane A and an abundance of particles in lane B. Therefore, the average density in lane A is always lower than the average density in lane B. An interesting observation is that whenever shock occurs in both the lanes, one cannot get a density profile of the kind shown in Fig. 7(a), as such a profile violates the condition $\rho_A < \rho_B$. One can infer from the above reasoning that shock in lane A is always to the right of the shock in lane B.

Figure 7(b) shows the variation in the distance between shocks in lane A and lane B with respect to Ω_A for different system sizes. Note that $\Omega_B = 0.25\Omega_A$, which means that both lane-changing rates grow together. Clearly, for small values of Ω_A, there is a significant difference between the positions of the two respective shocks, denoted by $x_{s,A} - x_{s,B}$ for all system sizes. Here $x_{s,j}$ denotes the position of the shock in lane j. For small values of Ω_A, the intershock distance $x_{s,A} - x_{s,B}$ is quite small and approaches zero on further increasing Ω_A. The order of the lane-changing rates, where $x_{s,A} - x_{s,B} \sim 0$, is referred to as the order of synchronization, which is found to be $100O(\Omega_d)$. Clearly, the system size has no effect on the order of synchronization.

For $O(\Omega_{A,B}) < 100O(\Omega_d)$, the shocks or domain walls (DWs) in the two lanes appear at different positions in the bulk, as clear from Figs. 8(a) and 8(b). On increasing the lane-changing rates, the shock in lane A moves leftward while the shock in lane B moves rightward. As soon as the order

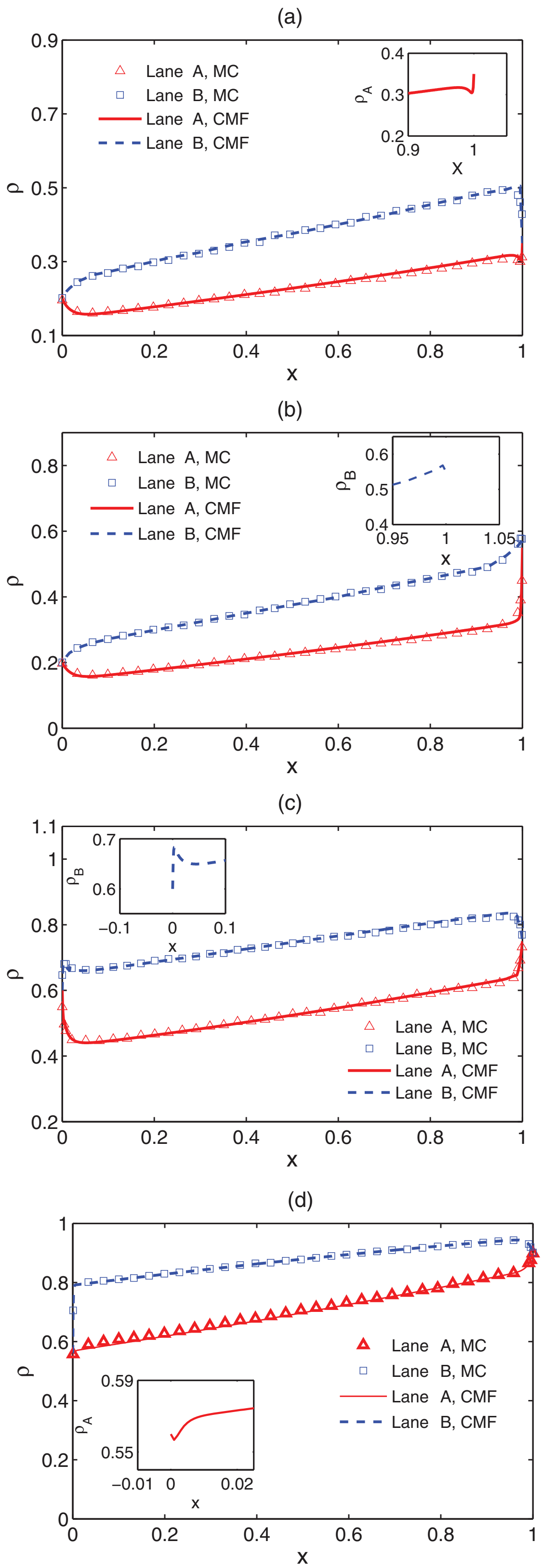

FIG. 6. (Color online) Density profiles in (a) region I, $\alpha = 0.2, \gamma = 0.35$, with a kink at the RBL in lane A; (b) region II, $\alpha = 0.2, \gamma = 0.55$, with a kink at the RBL in lane B; (c) regioin III, $\alpha = 0.6, \gamma = 0.75$, with a kink at the LBL in lane B; and (d) region IV, $\alpha = 0.56, \gamma = 0.9$, with a kink at the LBL in lane A. The respective insets show the kinks with magnification.

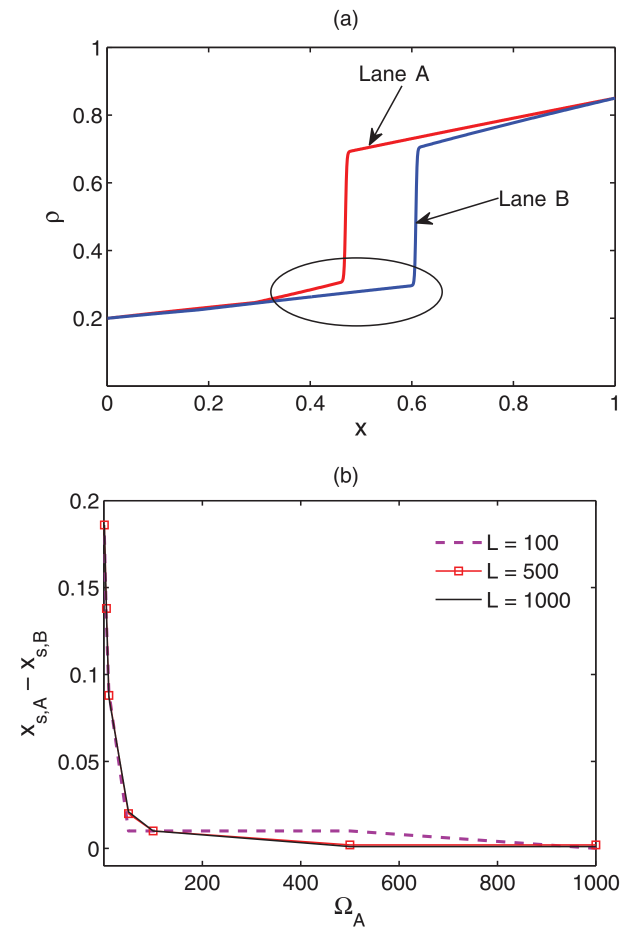

FIG. 7. (Color online) (a) Density profiles having shock in both lanes violating the condition $\rho_A < \rho_B$. The circled region shows a part of the lattice where $\rho_A > \rho_B$. (b) Distance between shocks vs Ω_A, where $\Omega_B = 0.25\Omega_A$ and $\Omega_a = \Omega_d = 0.2$.

of the lane-changing rates reaches $100O(\Omega_d)$, the positions of the shocks in both lanes almost match [see Fig. 8(c)], which is referred to as synchronization of shocks. We find that shocks are completely synchronized when $O(\Omega_{A,B}) = 1000O(\Omega_d)$ [Fig. 8(d)]. Moreover, after synchronization the two shocks move in the same direction in the bulk with respect to any further increase in lane-changing rates.

The synchronization occurs due to the gradually decreasing distance between the shocks as Ω_A and Ω_B grow. This phenomenon has also been observed in the past. In Ref. [35], Mitsudo and Hayakawa found that kinks (shocks) in two lanes become synchronized in a two-lane asymmetric simple exclusion process model without Langmuir kinetics. Later, Jiang *et al.* [30] introduced Langmuir kinetics into one of the lanes of a two-lane system. Although the lane-changing rates in the two-lane model of Jiang *et al.* [30] are symmetric, the dynamics of the particle attachment and detachment in exactly one of the two lanes imparts asymmetry to their model. Jiang *et al.* [30] found that synchronization of shocks in both lanes occurs when the lane-changing rate exceeds a specific threshold value. Interestingly, the threshold value specified in [30] is $\Omega_c = 10$, which has the same order as the one observed for our asymmetrically coupled system. The matching of order

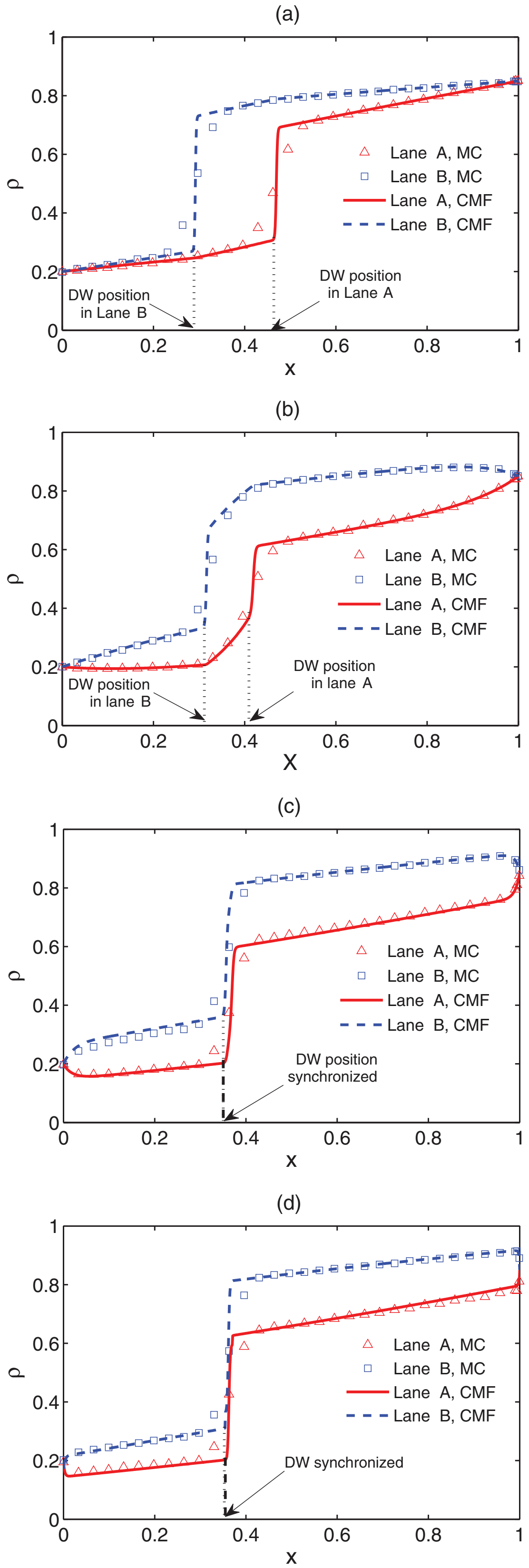

FIG. 8. (Color online) Density profiles in the (S,S) phase for $\alpha = 0.2$, $\gamma = 0.85$, and $\Omega_a = \Omega_d = 0.2$ with (a) $\Omega_A = 0.8$, $\Omega_B = 0.2$, (b) $\Omega_A = 8$, $\Omega_B = 2$, (c) $\Omega_A = 80$, $\Omega_B = 20$, and (d) $\Omega_A = 800$, $\Omega_B = 200$. Clearly, synchronization of the DWs occurs for $O(\Omega_{A,B}) \geqslant 100 O(\Omega_{a,d})$.

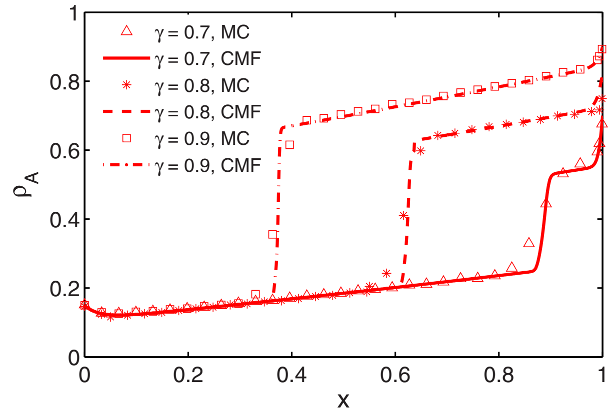

FIG. 9. (Color online) Effect of increasing γ on the height and position of shock in lane A for $\alpha = 0.15$, $\Omega_a = \Omega_d = 0.2$, $\Omega_A = 80$, and $\Omega_B = 20$.

of the threshold value of the lane-changing rates indicates that synchronization of shocks is one of the characteristics of two-lane particle nonconserving TASEPs.

In addition to its dependence on the order of lane-changing rates, the phenomenon of synchronization also depends on the ratio of the lane-changing rates. We have seen that synchronization of shocks does not occur when Ω_B/Ω_A is quite small, even for higher order of Ω_A. Our present study focuses on the fixed ratio of lane-changing rates ($\Omega_B/\Omega_A = 0.25$).

Figure 9 depicts that for fixed α, an increase in γ not only increases the height of the domain wall (shock) in lane A but also shifts its location leftward in the bulk. Physically, increasing γ means decreasing removal rate β, which leads to an increase in the density of particles at the right boundary and hence the HD portion of the shock profile moves to a higher magnitude and extends over a larger number of lattice sites. For the sake of clarity, we have given shock profiles in lane A only. The shock in lane B, which is at the same position as the shock in lane A, also shows similar dynamics due to the phenomenon of synchronization.

C. Disappearance of (LD,S) and (S,HD) phases

An important noteworthy aspect of the phase diagram [Fig. 4(b)] is that our system cannot exist in the (LD,S) and (S,HD) phases. The reason for the nonexistence of these two phases can be attributed to the synchronization of domain walls in both lanes, which restrains the two domain walls to occupy the same position in the bulk. So, their deconfinement from the boundary (either right or left) also occurs simultaneously. Thus, the domain wall cannot be present in the bulk (shock) in one lane while it is at the boundary in other lane. In this way, we cannot have (LD,S) and (S,HD) phases in the phase diagram.

As mentioned earlier, the synchronization of shocks does not occur for a small ratio of lane-changing rates. As a result, both (LD,S) and (S,HD) phases exist when Ω_B/Ω_A is small. This observation is consistent with the results obtained in [14], where we see the existence of (LD,S) and (S,HD) phases with $\Omega_B/\Omega_A \leqslant 0.1$ for any order of Ω_A. Although the model

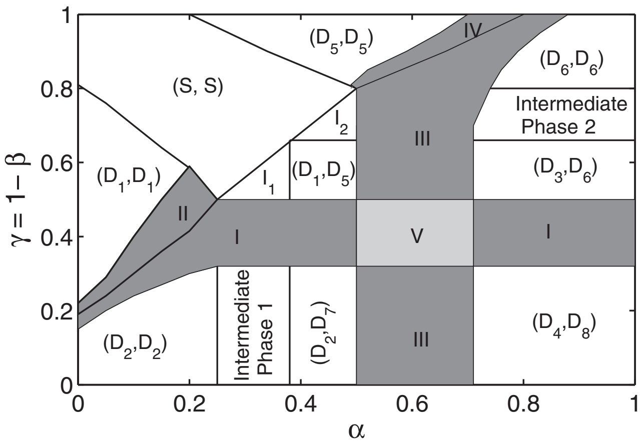

FIG. 10. Phase diagram with $\Omega_A = 800$ and $\Omega_B = 200$. The notation is the same as in Fig. 4(a).

studied in [14] is a two-channel TASEP without LK, it is reasonable to compare it with our model because $O(\Omega_{A,B}) = 100O(\Omega_{a,d})$ in our case.

The aforementioned distinguishing features of steady-state dynamics are preserved for the case when $O(\Omega_A) = O(\Omega_B) = 1000O(\Omega_d)$. Figure 10 shows the steady-state phase diagram with $\Omega_A = 800$ and $\Omega_B = 200$. The regions of surface transitions, denoted by I, II, III, and IV, have enlarged as a result of increasing lane-changing rates. Moreover, regions I and II and regions III and IV merge (but do not overlap) in such a way that leads to the extinction of two phases, namely, (tanh $-$ r,coth $-$ r) and (coth $-$ l,tanh $-$ l). There is no other noticeable change in the composition of the phase diagram. We have also investigated the effect of the system size on our results and observed that the bulk solution given by Monte Carlo simulations is independent of the lattice size. It is clear from Fig. 11(a) that the sharpness in the steep rise of the shock increases as one increases the number of lattice sites. For the sake of clarity, average densities in only one of the two lanes, viz., lane A, are shown. These observations are consistent with the results reported in the literature [31]. Figure 11(b) shows that the kink at the boundary layer emerges more clearly with an increase in the number of lattice sites, which also justifies that the system size chosen by us, viz., $L = 1000$, is appropriate to study such a system.

V. COMPARISON OF PARTIALLY ASYMMETRIC WITH FULLY ASYMMETRIC COUPLING CONDITIONS

As mentioned earlier, there are no structural differences between the phase diagrams under fully and partially asymmetric coupling conditions until $O(\Omega_{A,B}) < 100O(\Omega_{a,d})$. The density profiles also show a continuous transition as one moves from zero asymmetry (symmetric) to maximum asymmetry (fully asymmetric) via partially asymmetry. Figure 12(a) shows the variation in density profile in the (LD,S) phase for different values of lane-changing rates having order consistent with that of detachment-attachment rates. Clearly, the shape of the density profile does not change with a variation in the magnitude of Ω_B. Similarly, the other phases also preserve

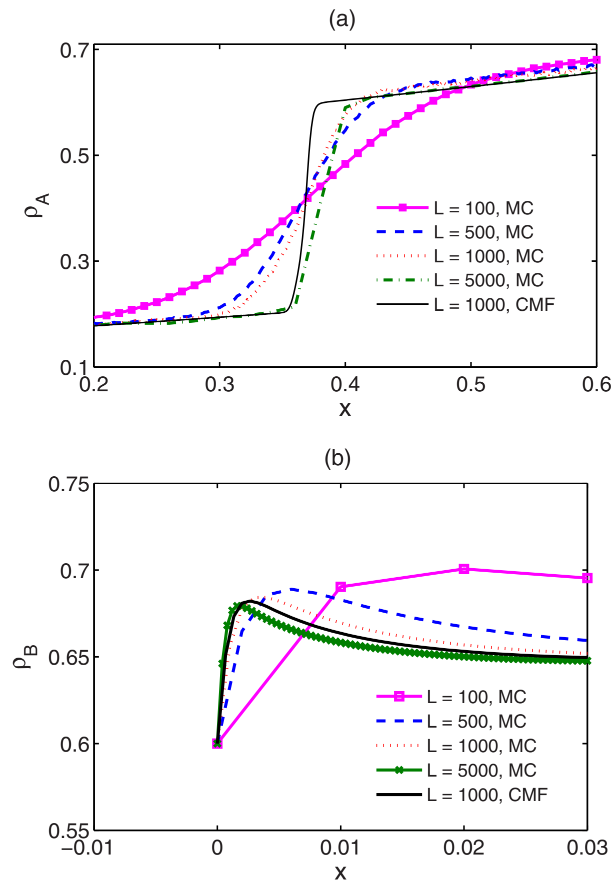

FIG. 11. (Color online) Effect of system size on the (a) shock profile and (b) kink in the boundary layer.

the shapes of density profiles. Moreover, there is no sudden appearance or disappearance of any phase in the phase plane. Thus, one can conclude that the consistency is preserved while moving between different coupling conditions for $O(\Omega_{A,B}) < 100O(\Omega_{a,d})$.

The above inference does not hold true for higher orders of lane-changing rates, i.e., $O(\Omega_{A,B}) \geqslant 100O(\Omega_{a,d})$. Here the phase diagrams of the system in fully and partially asymmetric coupling conditions are topologically different. Although the number of phases in phase diagrams with $\Omega_A = 100$, $\Omega_B = 0$ [32] and $\Omega_A = 80$, $\Omega_B = 20$ is the same, the nature of the phases differs. Importantly, we have seen that the two phases (LD,S) and (S,HD), which cover a considerable portion of the phase plane for $\Omega_A = 100$ and $\Omega_B = 0$, do not even exist for $\Omega_B \neq 0$. It is evident from Fig. 12(b) that the density profiles in lane B suddenly incur a shock as soon as $\Omega_B = 0$. Thus, we can conclude that there is a loss of consistency in the structure of the phase diagram as one shifts from partially asymmetric to fully asymmetric coupling conditions for higher orders of lane-changing rates. The disappearance of (LD,S) and (S,HD) phases does not happen abruptly when Ω_B takes a nonzero value. While Ω_A is fixed, a gradual increase in Ω_B leads to shrinkage of the (LD,S) and (S,HD) phases, which ultimately disappear for a certain value of Ω_B.

The aforementioned observations can be understood as follows. It is well known in the literature that for a

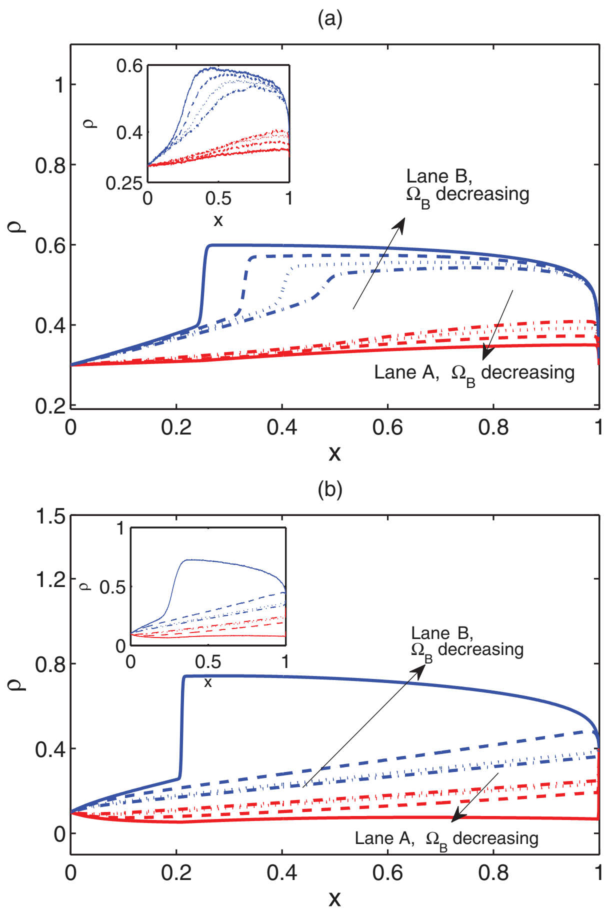

FIG. 12. (Color online) Transition of density profiles in both lanes for (a) $\Omega_A = 1$ and $\Omega_B = 0$, 0.1, 0.2, and 0.3 with $\alpha = 0.3$ and $\gamma = 0.3$ and (b) $\Omega_A = 100$ and $\Omega_B = 0$, 10, 30, and 40 with $\alpha = 0.1$ and $\gamma = 0.4$. The respective insets show the Monte Carlo simulations results, which indicate similar transitions in both cases.

two-lane TASEP without LK there are significant differences in the phase diagrams under fully asymmetric and partially asymmetric coupling conditions [23,24,29]. For $O(\Omega_{A,B}) \geqslant 100O(\Omega_{a,d})$, the effect of attachment and detachment is quite small as compared to lane changing, due to which the steady-state dynamics show a significant variation in partially and fully asymmetric coupling environments, parallel to the case of a two-lane TASEP without LK.

VI. CONCLUSION

In this work we have studied a two-lane totally asymmetric simple exclusion process with Langmuir kinetics in both lanes under partially asymmetric coupling conditions. A detailed study of the steady-state properties of the system was carried out using a boundary layer analysis of the mean-field equations in the continuum limit. The phase diagrams were obtained and the effect of lane-changing rates was thoroughly investigated. We classified the phase diagrams in terms of the order of transition rates. When the order of the lane-changing rates was equal to or ten times the order of the attachment-detachment rates, the structure of the phase diagram was qualitatively similar to the one in fully asymmetric coupling conditions. As we increased the order of the lane-changing rates to 100 times the order of the attachment-detachment rates, we observed significant changes in the phase diagram. Instead of getting a line of surface transition, we obtained subregions of surface transition in the phase plane. In these subregions, the boundary layer was neither tanh type nor coth type, but involved a kink at the boundary. The second important feature of the phase diagram is the synchronization of shocks in two lanes, which was not observed for lower orders of lane-changing rates or in fully asymmetric coupling conditions. The third distinguishing characteristic of the phase diagram is the disappearance or appearance of certain phases. We have also examined the effect of the system size on the density profiles. The results of continuum mean-field equations agree well with Monte Carlo simulations.

This work is an attempt to provide completeness to the steady-state properties of a two-lane TASEP with LK in all possible coupling environments. The present study might help not only in understanding complex dynamics of motor proteins but also towards enhancement of one's insight into nonequilibrium statistical mechanics.

ACKNOWLEDGMENT

I.D. acknowledges CSIR, New Delhi, India, for providing financial support.

[1] C. T. MacDonald, J. H. Gibbs, and A. C. Pipkin, Biopolymers **6**, 1 (1968).
[2] L. B. Shaw, R. K. P. Zia, and K. H. Lee, Phys. Rev. E **68**, 021910 (2003).
[3] T. Chou and G. Lakatos, Phys. Rev. Lett. **93**, 198101 (2004).
[4] S. Klumpp and R. Lipowsky, J. Stat. Phys. **113**, 233 (2003).
[5] B. Widom, J. Viovy, and A. Defontaines, J. Phys. (France) I **1**, 1759 (1991).
[6] K. Nagel, Phys. Rev. E **53**, 4655 (1996).
[7] D. Chowdhury, L. Santen, and A. Schadschneider, Phys. Rep. **329**, 199 (2000).
[8] J. Krug, Phys. Rev. Lett. **67**, 1882 (1991).
[9] V. Popkov, J. Stat. Mech. (2007) P07003.
[10] J. Krug, Braz. J. Phys. **30**, 97 (2000).
[11] M. Clincy, M. R. Evans, and D. Mukamel, J. Phys. A: Math. Gen. **34**, 9923 (2001).
[12] M. R. Evans, R. Juhasz, and L. Santen, Phys. Rev. E **68**, 026117 (2003).
[13] V. Popkov, A. Rákos, R. D. Willmann, A. B. Kolomeisky, and G. M. Schütz, Phys. Rev. E **67**, 066117 (2003).
[14] R. Jiang, M.-B. Hu, Y.-H. Wu, and Q.-S. Wu, Phys. Rev. E **77**, 041128 (2008).
[15] J. Howard, *Mechanics of Motor Proteins and the Cytoskeleton* (Sinauer, Sunderland, MA, 2001).
[16] N. Mirin and A. B. Kolomeisky, J. Stat. Phys. **110**, 811 (2003).

[17] A. Parmeggiani, T. Franosch, and E. Frey, Phys. Rev. E **70**, 046101 (2004).
[18] A. Parmeggiani, T. Franosch, and E. Frey, Phys. Rev. Lett. **90**, 086601 (2003).
[19] S. Mukherji and V. Mishra, Phys. Rev. E **74**, 011116 (2006).
[20] E. Pronina and A. B. Kolomeisky, J. Phys. A: Math. Gen. **37**, 9907 (2004).
[21] E. Pronina and A. B. Kolomeisky, Physica A **372**, 12 (2006).
[22] E. Pronina and A. B. Kolomeisky, J. Phys. A: Math. Theor. **40**, 2275 (2007).
[23] K. Tsekouras and A. B. Kolomeisky, J. Phys. A: Math. Theor. **41**, 465001 (2008).
[24] Q.-H. Shi, R. Jiang, M.-B. Hu, and Q.-S. Wu, J. Stat. Phys. **142**, 616 (2011).
[25] Q.-H. Shi, R. Jiang, M.-B. Hu, and Q.-S. Wu, Phys. Lett. A **376**, 2640 (2012).
[26] B. Saha and S. Mukherji, J. Stat. Mech. (2013) P09004.
[27] M. R. Evans, Y. Kafri, K. Sugden, and J. Tailleur, J. Stat. Mech. (2011) P06009.
[28] V. Yadav, R. Singh, and S. Mukherji, J. Stat. Mech. (2012) P04004.
[29] A. K. Gupta and I. Dhiman, Physica A **392**, 6314 (2013).
[30] R. Jiang, R. Wang, and Q.-S. Wu, Physica A **375**, 247 (2007).
[31] R. Wang, R. Jiang, M. Liu, J. Liu, and Q.-S. Wu, Int. J. Mod. Phys. C **18**, 1483 (2007).
[32] A. K. Gupta and I. Dhiman, Phys. Rev. E **89**, 022131 (2014).
[33] J. D. Cole, *Perturbation Methods in Applied Mathematics* (Blaisdell, Waltham, 1968).
[34] S. Mukherji and S. M. Bhattacharjee, J. Phys. A: Math. Gen. **38**, L285 (2005).
[35] T. Mitsudo and H. Hayakawa, J. Phys. A: Math. Gen. **38**, 3087 (2005).